

## Analysis of signal propagation in optically coupled detectors for digital mammography: II. Lens and fibre optics

This content has been downloaded from IOPscience. Please scroll down to see the full text.

1996 Phys. Med. Biol. 41 475

(<http://iopscience.iop.org/0031-9155/41/3/010>)

View [the table of contents for this issue](#), or go to the [journal homepage](#) for more

Download details:

IP Address: 170.212.0.65

This content was downloaded on 15/07/2016 at 18:42

Please note that [terms and conditions apply](#).

## Analysis of signal propagation in optically coupled detectors for digital mammography: II. Lens and fibre optics\*

Andrew D A Maidment† and Martin J Yaffe

Departments of Medical Biophysics and Radiology, University of Toronto, and Research Division, Sunnybrook Health Science Centre 2075 Bayview Avenue Toronto, Ontario M4N 3M5, Canada

Received 28 March 1995, in final form 3 November 1995

**Abstract.** An x-ray detector for digital x-ray mammography is under investigation, which consists of a phosphor screen coupled by a demagnifying fibre-optic taper to a time-delay integration mode, charge-coupled device (CCD) image array. The signal propagation through such a detector depends on the intensity and angular emission of light from the phosphor screen, the angular acceptance and transmission of light through the optics, and the spectral sensitivity of the CCD to the fluorescent light. The production of light by the phosphor screen was considered in a previous paper. Here, the issues related to the optics are examined. For phosphor screens coupled by lenses with limiting acceptance angles of less than  $30^\circ$ , it was calculated that the coupling efficiency would be 10% greater than would be estimated under the assumption of a Lambertian source. These increases occur because a phosphor screen typically produces light which is more forward directed than a Lambertian source. Similar increases in efficiency are observed when a phosphor screen is coupled to a fibre-optic faceplate or taper. For fibre optics, exact estimation of the optical coupling efficiency requires knowledge of the angular-dependent transmission efficiency of the fibres.

### 1. Introduction

A digital radiographic imaging system has been developed at the University of Toronto for use in full-field digital mammography (Maidment 1993, Maidment *et al* 1993). The imaging system consists of a mammographic phosphor screen which is coupled via a fibre-optic taper to a time-delay integration mode charge-coupled device (CCD) image array. We refer to these devices as phosphor–optics–CCD (POC) detectors. In POC detectors, the signal-to-noise ratio (SNR) is determined, in part, by the efficiency with which light quanta produced in a phosphor screen are recorded (Albrecht 1965, Fu 1984, Rabbani *et al* 1987, Rabbani and VanMetter 1989, Nishikawa and Yaffe 1990, VanMetter and Rabbani 1990, Maidment and Yaffe 1994). In this paper, we present a method to calculate the efficiency of the optical coupling of a phosphor screen to the CCD image array.

Three representative POC image detectors are illustrated in figure 1. All three detectors use a single optical component to convey light from a phosphor screen to a CCD image array. In figure 1(a) the optical coupling is provided by a relay lens, while a Bouwer's

\* Presented in part at the *Young Investigators Symp., 34th Annu. Meeting AAPM (Calgary, 1992)*.

† Current address: Department of Radiology, Thomas Jefferson University, 3390 Gibbon Building, 111 South 11th Street, Philadelphia, PA 19107-5098, USA.

reflective lens is used in figure 1(b). These two lenses are typical of those used in early videofluoroscopy systems (Ter-Pogossian 1967), from which concerns regarding SNR degradation stimulated the design of high-efficiency optics. The former approach has been used by Karellas *et al* (1992) in the design of small field-of-view digital mammography imaging systems, while the latter approach has been used by Andre *et al* (1994) in the design of a full-field-of-view digital mammography imaging system. In figure 1(c), a demagnifying fibre-optic taper is shown. Such fused fibre-optic arrays, developed by Kapany (1955), have the potential to provide far greater optical coupling efficiencies than are possible with lenses, because of their large acceptance solid angle. As discussed below, a fibre-optic taper can provide a twofold to sixfold increase in optical coupling as compared to lenses, assuming both systems are well designed.

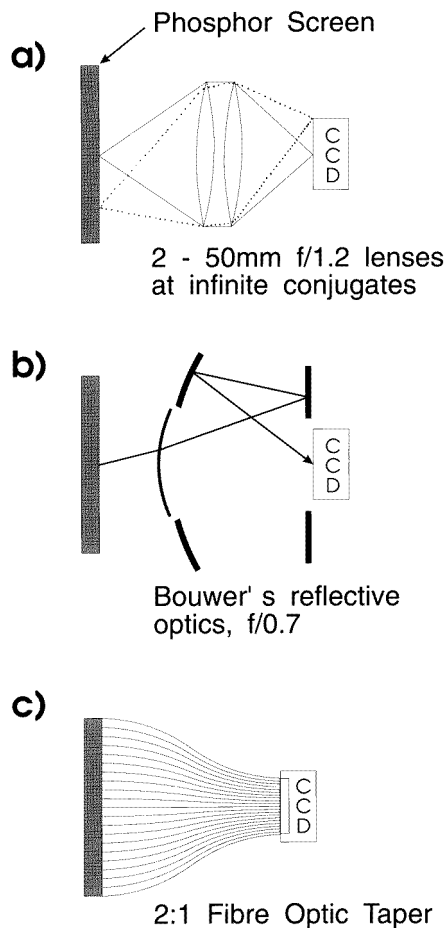


**Figure 1.** Three POC detectors are shown. In each case, a phosphor screen is optically coupled to a CCD image array. The optical coupling consists of (a) relay lenses, (b) Bouwer's reflective optics, and (c) a fused fibre-optic taper.

The POC detectors presented in figure 1 are examples of the more general  $n$ -stage cascaded POC detectors considered below. The components of POC detectors can be treated as consisting of serially cascaded elements which propagate x-ray, light, or electron

images. We have previously presented a method of analysing the absorption of x-rays and the generation of light quanta in phosphors, including a model for calculating the angular emission of light (Maidment and Yaffe 1995). In this paper, the angular-dependent propagation of light through lenses and fused fibre-optic arrays is reviewed. Means of simplifying this analysis to handle the special cases of illumination by a Lambertian source and propagation of meridional rays are demonstrated to clarify the assumptions implicit in these well known relationships and to illustrate their limitations. Experimental measurement of the optical properties of fibre optic faceplates typical of those used in POC detectors is described. These analyses provide tools to allow one to calculate the 'total coupling efficiency' of the detector, which is specified as the number of electrons generated in the CCD per x-ray interaction in the phosphor screen. A discussion of lenses and fibre optics is presented to facilitate comparison of the design of POC detectors. Such a comparison requires the calculation of total coupling efficiency, which is described in more detail by Maidment (1993). The total coupling efficiency is, in turn, a prerequisite for calculating the detective quantum efficiency (DQE) of POC detectors (Maidment and Yaffe 1994).

## 2. Theory

The coupling efficiency,  $\xi$ , of a lens or an optical fibre is given by the ratio of the acceptance solid angle to the solid angle of a hemisphere, weighted by the radiant intensity of the incident light,  $J_i(\theta_i, \phi_i)$ , and the transmission efficiency,  $\tau(\theta_i, \phi_i)$ . The transmission coefficient accounts for both reflective and absorptive losses. The coupling efficiency is given by

$$\xi = \int_0^{2\pi} \int_0^{\theta_{i,M}} J_i(\theta_i, \phi_i) \tau(\theta_i, \phi_i) \sin(\theta_i) d\theta_i d\phi_i / \int_0^{2\pi} \int_0^{\pi/2} J_i(\theta_i, \phi_i) \sin(\theta_i) d\theta_i d\phi_i. \quad (1)$$

The differential solid angle is given by  $\sin(\theta_i)d\theta_id\phi_i$ , where  $\theta_i$  is the incident meridional angle,  $\phi_i$  is the incident azimuthal angle, and  $\theta_{i,M}$  is the meridional angle that the marginal ray makes with the principal axis<sup>†</sup>. In this paper, it is assumed that the optics are axially symmetric, hence, all quantities below will be specified as functions of  $\theta_i$  only. Thus, equation (1) is simplified.

Coupling several optical elements requires one to consider how the light is emitted from the previous element, and how the light is collected by the following element. In the absence of scattering, the light emitted from an axially symmetric optical element at angle  $\theta_o$  is given by

$$J_o(\theta_o) = \begin{cases} J_i(\theta_i)\tau(\theta_i) & \theta_i \leq \theta_{i,M} \\ 0 & \text{otherwise} \end{cases} \quad (2)$$

where

$$\theta_o = \sin^{-1}(m(n_i/n_o) \sin(\theta_i)) \quad (3)$$

$m$  is the demagnification of the component, and  $n_i$  and  $n_o$  are the refractive indices of the input and output media. Using equations (1)–(3), it is possible to calculate the coupling efficiency of a series of lens and fibre optics.

<sup>†</sup> This formulation is appropriate for lenses and the meridional approximation of optical fibres. For the skew approximation,  $\theta_{i,M} = \pi/2$  regardless of the numerical aperture of the optical fibre.

## 2.1. Lenses

Consider the lens shown in figure 2(a). The coupling efficiency of the lens for light emitted from a point  $S_1$  on the principal axis is given by equation (1). Because the limiting meridional angle,  $\theta_M$ , of most lenses is small, equation (1) may be simplified by treating the transmission efficiency of the lens as being independent of angle (given by a constant,  $\tau$ ).

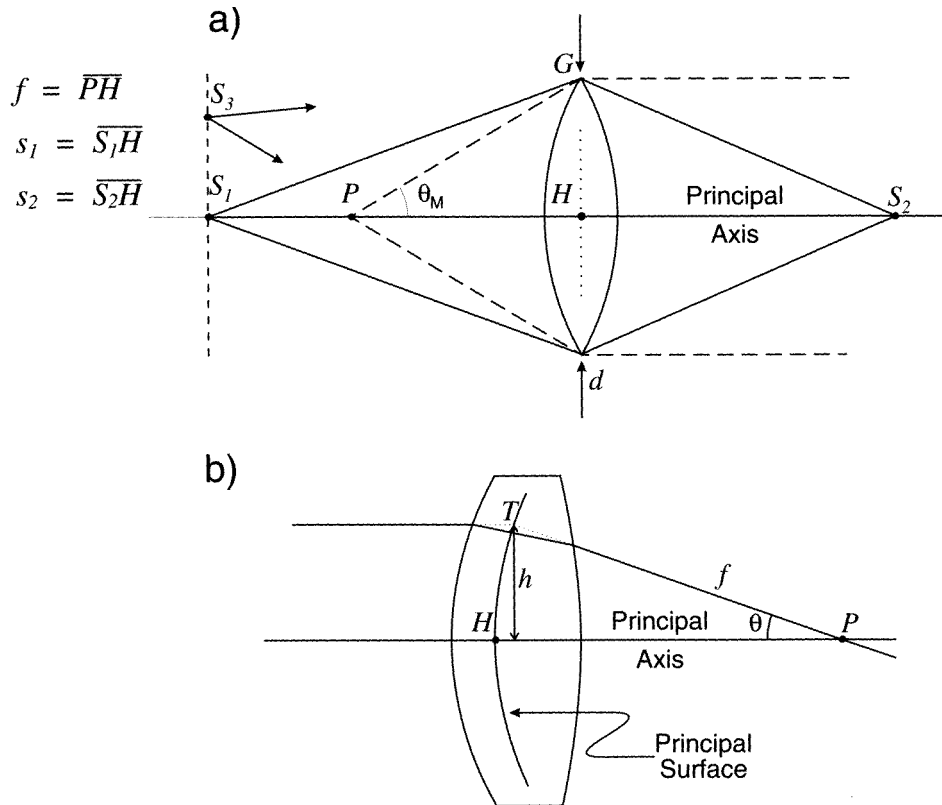


**Figure 2.** (a) A simplified schematic diagram of a single lens. The focal length,  $f$ , is given by the distance  $\overline{PH}$ . The limiting aperture diameter is  $d$ . A general point,  $S_1$ , is shown in focus with the conjugate,  $S_2$ . (b) The principal surface passing through points  $H$  and  $T$  in detail, illustrating how the conjugate rays are projected until intersection.

The coupling efficiency at point  $S_3$  off the principal axis may also be calculated using equation (1). However, the limiting meridional angle must be expressed as a function of the azimuthal angle. This calculation can be simplified if the light source is Lambertian. This assumption results in a dependence of off-axis irradiance which varies with the fourth power of the cosine of the angle of incidence (Boyd 1983, Kingslake 1983, pp 122–3). Vignetting (the result of a variation in the area of the limiting aperture as a function of angle of incidence of light) can cause additional off-axis signal reduction (Kingslake 1983, pp 85–6, 129–30).

**2.1.1. Lambertian light sources.** Because of the small value of the limiting meridional angle of most lenses, many light sources may be approximated as Lambertian. For a

Lambertian source,  $J_i(\theta_i) = J_0 \cos(\theta_i)$  for  $-\pi/2 \leq \theta_i \leq \pi/2$ , thus equation (1) gives

$$\xi = \tau \sin^2(\theta_M) \quad (4)$$

for a point on the principal axis. The value of  $\sin(\theta_M)$  can be related to the  $f$ -number of the lens by using fundamental optical definitions. There has been debate (Miller 1971) and continued interest (Munro *et al* 1990, Swindell 1991, Liu *et al* 1994) on the exact nature of this relationship. Consider the lens illustrated in figure 2(b). The  $f$ -number ( $F$ ) of the lens is the ratio of the focal length of the lens to the limiting aperture diameter. If light rays from the object originate at the focal point, P, then the conjugate rays must be parallel. If the light rays in the image space and object space are extended until they intersect, then the surface that is formed by the intersection of all such rays is called the principal surface (Born and Wolf 1989, pp 152–3). If an optical system is perfect†, well corrected and free of coma, then the principal surface is spherical due to the Abbe sine law (Born and Wolf 1989, pp 166–9, Jenkins and White 1957). Hence,

$$\sin(\theta_M) = d/2f = 1/2F \quad (5)$$

where the limiting aperture diameter,  $d$ , is the distance between the two opposed marginal meridional rays, and  $f$  is the focal length of the lens. This result differs from that of Liu *et al* (1994), who have approximated the principal surface as a plane. Such an approximation is valid for high  $f$ -number lenses, but will result in underestimation of limiting meridional angle and transmission efficiency for the low  $f$ -number lenses typically used in digital mammography.

In the general case, an object at point,  $S_1$ , will have an image at point  $S_2$ . Combining equation (5), the lens makers formula ( $1/f = 1/s_1 + 1/s_2$ ), and the demagnification ( $m = s_1/s_2$ ), gives

$$\sin(\theta_M) = d/2s_1 = 1/2F(m + 1) \quad (6)$$

where in this case  $\theta_M$  is the angle  $GS_1H$  in figure 2(a). Substituting equation (6) into equation (4) gives the coupling efficiency of a single lens,

$$\xi = \tau/4F^2(m + 1)^2. \quad (7)$$

Equation (7) is well known, and is valid for perfect, coma-free optics illuminated by a Lambertian source. The above derivation is valid for both the refractive and reflective lens systems illustrated in figure 1.

**2.1.2. Relay lenses.** A common method of coupling lenses in radiography involves relay lenses (Ter-Pogossian 1967, pp 349–55, Vermeulen *et al* 1982). Relay lenses are compound lenses consisting of two lenses (either refractive or reflective) applied at infinite conjugates, as illustrated in figure 3. The first lens (called the collimator) collimates the divergent beam of light emitted from the light source (typically a phosphor screen) into a parallel beam. The second lens (called the camera lens) focuses the light onto the detector. The coupling efficiency of relay lenses is also given by equation (7) if the lenses are perfect and free of coma and are illuminated by a Lambertian source and the following substitutions are applied. In this case, the transmission efficiency,  $\tau$ , is the product of  $\tau_{COL}$  and  $\tau_{CAM}$ , the transmission efficiencies of the two individual lenses. The focal length of the relay lens can be calculated using the lens law,

$$1/f = 1/f_{COL} + 1/f_{CAM} - l_r/f_{COL}f_{CAM}. \quad (8)$$

† A lens is considered perfect if any curve in the object space is geometrically similar to the image which is produced.

The distance between the points where the principal surfaces cross the principal axis,  $l_r$ , is usually small compared to the focal lengths of the individual lenses ( $f_{COL}$  and  $f_{CAM}$ ) and can be ignored. The diameter of the limiting aperture,  $d$ , is the lesser of  $d_{COL}$  and  $d_{CAM}$ . Finally, the demagnification,  $m$ , is defined as the ratio of the focal lengths of the individual lenses,  $m = f_{COL}/f_{CAM}$ .

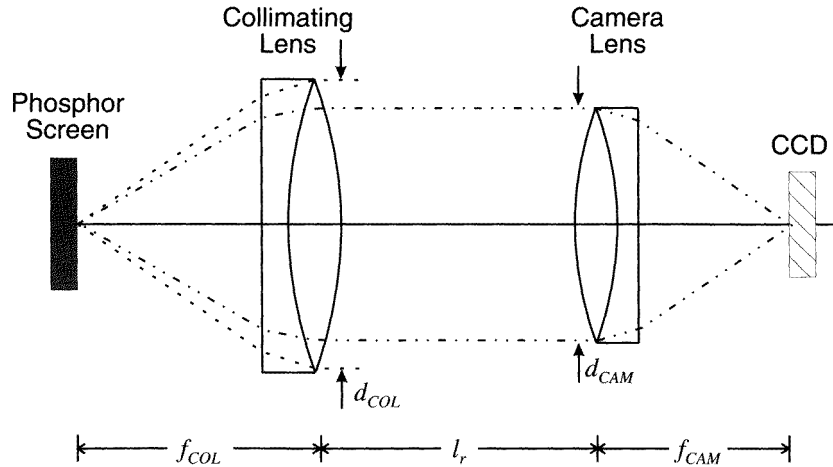


**Figure 3.** A schematic diagram of a relay lens showing the relationship between the collimating lens and the camera lens. The limiting aperture diameter of the relay lens is given by the smaller of  $d_{CAM}$  and  $d_{COL}$ .

## 2.2. Fibre optics

The propagation of light in single multimode optical fibres is well understood, and is readily predictable from geometric ray optics (Kapany 1967, Okashi 1982, Potter 1960). Calculations of the angular dependent transmission efficiency of optical fibres have been made on the basis of both meridional (Kapany 1967, Kapany and Capellaro 1961) and skew rays (Potter 1960, 1961, Potter *et al* 1963, Li and Lit 1985, Dugas *et al* 1987). The transmission properties of fused fibre-optic (FO) assemblies (e.g. faceplates and demagnifying tapers) may be similarly predicted (Kapany 1967).

As with lenses, equation (1) is used to calculate coupling efficiency. However, because of the large acceptance angles of optical fibres, the angular dependence of the factors within the integrals is important in calculating the true photometric efficiency of optical fibres. As noted by Kapany (1967, pp 160–1), the following factors affect the coupling efficiency of fibre optics: (i) fibre numerical aperture (NA); (ii) angular distribution of the incident light; (iii) bulk absorption coefficients of the core and cladding glass; (iv) the quality of the core–cladding interface; (v) core glass imperfections which cause light scattering; (vi) the cylindricity, curvature, and cross section of the fibres; and (vii) the packing efficiency of FO assemblies. Presented below are two models which can account for these factors through consideration of the bulk properties of the optical fibres.

**2.2.1. Meridional ray analysis.** In the meridional model, light rays incident with angle  $\theta_i$  in a plane containing the optical axis are considered to represent the propagation of all

light rays of similar angle, as shown in figure 4. The NA of the fibre is given by  $NA = (n_1^2 - n_2^2)^{1/2}$ , where  $n_1$  and  $n_2$  are the refractive indices of the core and cladding glass. The critical angle in the fibre is  $\phi_C = \sin^{-1}(n_2/n_1)$ . A light ray incident upon the fibre will undergo guided transmission if  $\theta_i \leq \theta_{i,M}$ , where the limiting meridional angle of incidence is  $\theta_{i,M} = \sin^{-1}(NA/n_i)$ . As seen in figure 4,  $\theta_{i,M}$  is related to  $\theta_{1,M}$  by Snell's law. The limiting meridional angle in the core glass,  $\theta_{1,M}$ , is equal to  $\pi/2 - \phi_C$ . Note that during passage through the fibre, the meridional angle is preserved due to total internal reflection.

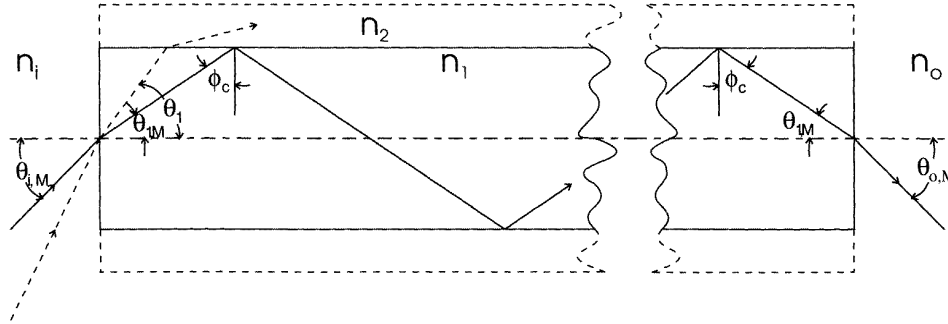


**Figure 4.** An optical fibre shown in cross section through the optical axis. Marked are the refractive indices of the entrance medium ( $n_i$ ), exit medium ( $n_o$ ), core glass ( $n_1$ ), and cladding glass ( $n_2$ ). Also shown are the critical angle ( $\phi_C$ ), and the limiting meridional angles ( $\theta_{i,M}$  and  $\theta_{1,M}$ ). An unreflected ray with angle  $\theta_1 > \theta_{1,M}$  is also shown (dashed line).

If the transmission efficiency of an optical fibre is independent of angle, and the fibre is illuminated by a Lambertian source, then the optical coupling efficiency is given by equation (4). This equation may also be expressed as  $\xi = \tau(NA)^2/n_i^2$ . This formulation is useful as a first-order approximation for calculating coupling efficiency; however, the transmission efficiency of most fibre optics cannot be represented as a constant.

Kapany and Capellaro (1961) provide a more accurate model, where the transmission efficiency of an optical fibre is given by

$$\tau_M(\theta_i) = T_{n_i, n_1}(\theta_i) e^{\alpha L \sec(\theta_1)} [1 - \bar{\beta}(\theta_1)]^{L \tan(\theta_1)/2a} T_{n_1, n_o}(\theta_1). \quad (9)$$

$\theta_i$  is the angle of a light quantum in the input medium which can be related to the angle of the light in the core glass,  $\theta_1$ , by Snell's law. The radius and length of the fibre are given by  $a$  and  $L$ ,  $\alpha$  is the bulk attenuation coefficient of the core glass,  $\bar{\beta}(\theta_1)$  is the average reflection loss per reflection with the cylinder wall, and  $L \tan(\theta_1)/2a$  is the number of internal reflections which occur for a ray with angle  $\theta_1$ . The Fresnel transmission factor for the transition between the input media and the core glass is  $T_{n_i, n_1}(\theta_i)$ , and that for the transition between the core glass and the exit media is  $T_{n_1, n_o}(\theta_1)$  (see equation (4) of Maidment and Yaffe (1995)). In equation (9),  $\bar{\beta}(\theta_1)$  typically has value of 0.001 or less for  $0 \leq \theta_1 \leq \theta_{1,M}$ , the range of angles for which total internal reflection occurs, while  $\bar{\beta}(\theta_1) = 1 - T_{n_1, n_2}(\pi/2 - \theta_1)$  for other values of  $\theta_1$ . Typical fibre diameters range from 5 to 10  $\mu\text{m}$ , thus even for a 1 mm thick FO assembly ( $L/2a = 50\text{--}100$ ) it is valid to use the approximation  $\bar{\beta}(\theta_1) = 1$  for  $\theta_{1,M} < \theta_1 \leq \pi/2$ . This leads to a discontinuity in  $\tau$  at  $\theta_1 = \theta_{1,M}$ , because beyond this angle total internal reflection will no longer occur.

Consider a 6 mm long, 0.005 mm diameter circular optical fibre with  $n_1 = 1.62$  and  $n_2 = 1.50$ , held in air (i.e.,  $n_i = n_o = 1.0$ ). In figure 5(a), the effect of bulk attenuation

on the transmission efficiency of this fibre is illustrated. The results are calculated from equation (9) for various values of  $\alpha$  (in  $\text{mm}^{-1}$ ), with  $\bar{\beta} = 0$ . In figure 5(b), the effect of reflection losses is illustrated by varying the value of  $\bar{\beta}$  with  $\alpha = 0$ . In both figures, Fresnel losses at the entrance and exit reduce transmission by 11% at  $\theta_i = 0$ . In figure 5(a), non-zero values of  $\alpha$  result in a transmission reduction at all angles, with only a slight dependence on  $\theta_i$ . In figure 5(b), non-zero values of  $\bar{\beta}$  do not affect transmission at  $\theta_i = 0$ , but reduce transmission at larger angles with a strong dependence on  $\theta_i$ .

2.2.2. *Skew ray analysis.* Kapany and Capellaro (1961) and Potter (1961) have also calculated the transmission of arbitrary (skew) rays through a perfect cylindrical fibre. To illustrate a portion of the path of a skew ray, an optical fibre is shown in figure 6 in perspective and in projection of the cross section. An incident skew ray, shown in the plane KLP, strikes the fibre wall at an angle  $\psi$  to the normal (a vector parallel to OP passing through point L). The ray is reflected into the plane PLM. It has been shown (Potter 1961) that  $\cos(\psi) = \sin(\theta_1) \cos(\gamma)$ , where  $\theta_1$  is the meridional angle and  $\gamma$  is the azimuthal (skew) angle. Using this relationship, Potter has shown that an incident ray will undergo guided transmission if  $\sin(\theta_1) \cos(\gamma) \leq \text{NA}/n_i$ . Note that the magnitudes of both the meridional and azimuthal angles are preserved upon reflection. Potter has shown that guided transmission of arbitrary rays occurs for the range of angles  $\bar{\gamma}(\theta_1) \leq \gamma \leq \pi/2$ , where

$$\begin{aligned} \bar{\gamma} &= 0 & \text{for } 0 \leq \theta_1 \leq \theta_{1,M} \\ \bar{\gamma} &= \cos^{-1}[\sin(\theta_{1,M})/\sin(\theta_1)] & \text{for } \theta_{1,M} < \theta_1 \leq \pi/2. \end{aligned} \quad (10)$$

Note that all meridional rays have  $\gamma = 0$ , hence meridional rays are a subset of skew rays.

Using a skew ray model, Potter (1961) has calculated that the transmission efficiency is given by

$$\tau_s(\theta_i) = \frac{4}{\pi} T_{n_i, n_1}(\theta_i) e^{-\alpha L \sec(\theta_1)} T_{n_i, n_o}(\theta_1) \int_{\bar{\gamma}(\theta_1)}^{\pi/2} [1 - \bar{\beta}(\psi)]^{L \tan(\theta_1)/2a \cos(\gamma)} \cos^2(\gamma) d\gamma. \quad (11)$$

This modification takes into account the fact that the skew rays will undergo more reflections with the wall than will meridional rays. Thus, the transmission efficiency at an angle  $\theta_i$  must be integrated over all of the values of the skew angle,  $\gamma$ . The skew angle must in turn be related to the fractional area of the fibre for which guided transmission of the incident skew light will occur. Thus, the differential area element,  $dA = \cos(\gamma)^2 d\gamma$ , is expressed as a function of the skew angle (Potter 1960). Note that  $\bar{\beta}$  is stated as a function of  $\psi$ , the angle between the normal to the point of interaction with the fibre wall and the incident ray, which for meridional rays is equal to  $\theta_1$ .

In figure 7, a 6 mm long, 0.005 mm diameter circular optical fibre with  $n_1 = 1.62$  and  $n_2 = 1.50$ , held in air, is once again considered. In figure 7(a), the effect of bulk attenuation on the transmission efficiency of this fibre is illustrated. The results are calculated for various values of  $\alpha$  (in  $\text{mm}^{-1}$ ), with  $\bar{\beta} = 0$ . In figure 7(b), the effect of reflection losses is illustrated by varying the value of  $\bar{\beta}$  with  $\alpha = 0$ . As with the meridional model, Fresnel losses at the entrance and exit reduce transmission by 11% at  $\theta_i = 0$ . In figure 7(a), non-zero values of  $\alpha$  result in a transmission reduction at all angles, with only a slight dependence on  $\theta_i$ . The large reduction in transmission efficiency for  $\theta_i > \theta_{i,M}$  is due to the reduced acceptance area for skew rays. As in the meridional model, non-zero values of  $\bar{\beta}$  (figure 7(b)) do not affect transmission at  $\theta_i = 0$ , but do result in reduction of transmission at higher angles with a strong dependence on  $\theta_i$ . Note that the value of  $\tau_s(\theta) > \tau_M(\theta)$  due to the transmission of skew rays.

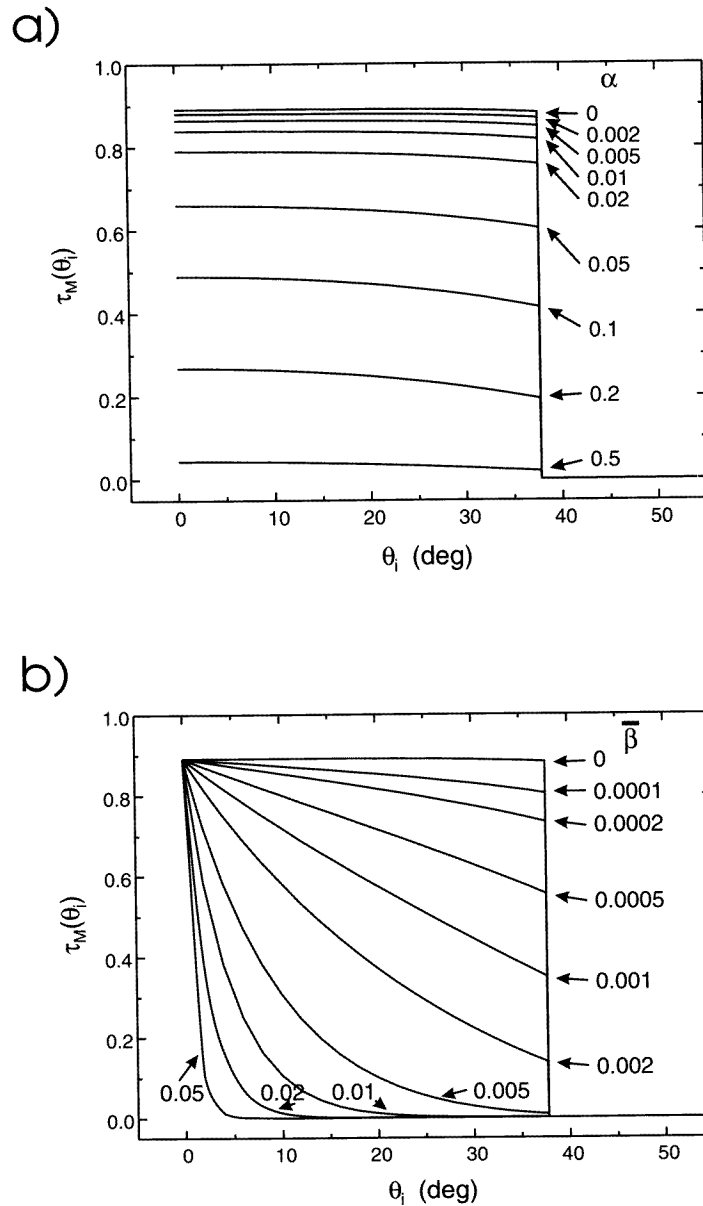


**Figure 5.** The results of the meridional ray hypothesis calculated using equation (9), (a) for different values of  $\alpha$ , assuming  $\bar{\beta} = 0$ , and (b) for different values of  $\bar{\beta}$ , assuming  $\alpha = 0$ . The calculations were performed using  $L = 6$  mm,  $n_1 = 1.62$ , and  $n_2 = 1.50$ , giving an optical fibre with NA = 0.61. The values of  $\alpha$  are given in  $\text{mm}^{-1}$ .

In perfect cylindrical fibres, both  $\theta$  and  $\gamma$  of the skew ray model are preserved on passage through the fibre. In imperfect fibres, skew rays with  $\theta_1 > \theta_{1,M}$  will be removed since  $\gamma$  is not preserved. Hence, for long single fibres with irregular cross section, the meridional approximation will be accurate. This is in agreement with the experimental findings of Dugas and co-workers (1987).

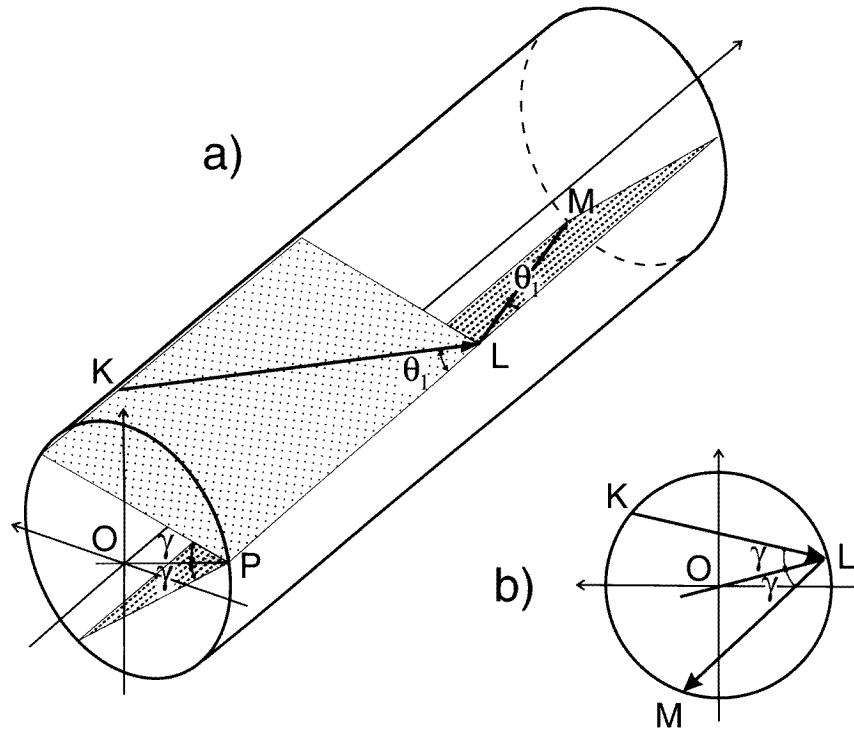


**Figure 6.** An optical fibre shown in perspective and in projection. Shown is a skew ray reflecting off the core-cladding interface with meridional angle  $\theta_1$  and skew angle  $\gamma$ . The skew angle is the angle between the plane of the ray and the plane containing the optical axis and the normal to the cylinder at the point of reflection.

**2.2.3. Fused FO assemblies.** To provide a practical optical coupling, a fused assembly of optical fibres is required. The transmission efficiency of a fused FO assembly at an angle  $\theta_i$  is the product of the fractional area of the core glass ( $A$ ) and the transmission efficiency of the individual fibres which may be calculated using either equation (9) or (11).

An image may be demagnified using a fused FO taper. In tapered optical fibres, the limiting meridional angle is specified by  $\sin(\theta_{i,M}) = (n_1^2 - n_2^2)^{1/2} / (n_i m)$ . The demagnification,  $m$ , is given by the ratio of the input fibre diameter to the output fibre diameter. These results are based upon the propagation of meridional rays in a cone with axial length many times greater than the diameter (Kapany 1967, pp 18–22). For the simplified situation of a Lambertian source and  $\tau$  constant, the effect of demagnification is to reduce the coupling efficiency of the optical fibre by a factor of  $m^2$ .

In FO arrays, the juxtaposition of fibres means that light which is removed from one optical fibre will travel unguided some distance laterally before (i) leaving the faceplate, (ii) being attenuated by the cladding or core glass, or (iii) continuing guided transmission in an adjacent fibre. Light which enters the cladding glass rather than the core glass may not be rapidly attenuated. It is for this reason that extramural absorption (EMA) materials are included in fused FO arrays. Measurements of the angular dependence of transmission efficiency of fused FO arrays with and without EMA are described below.

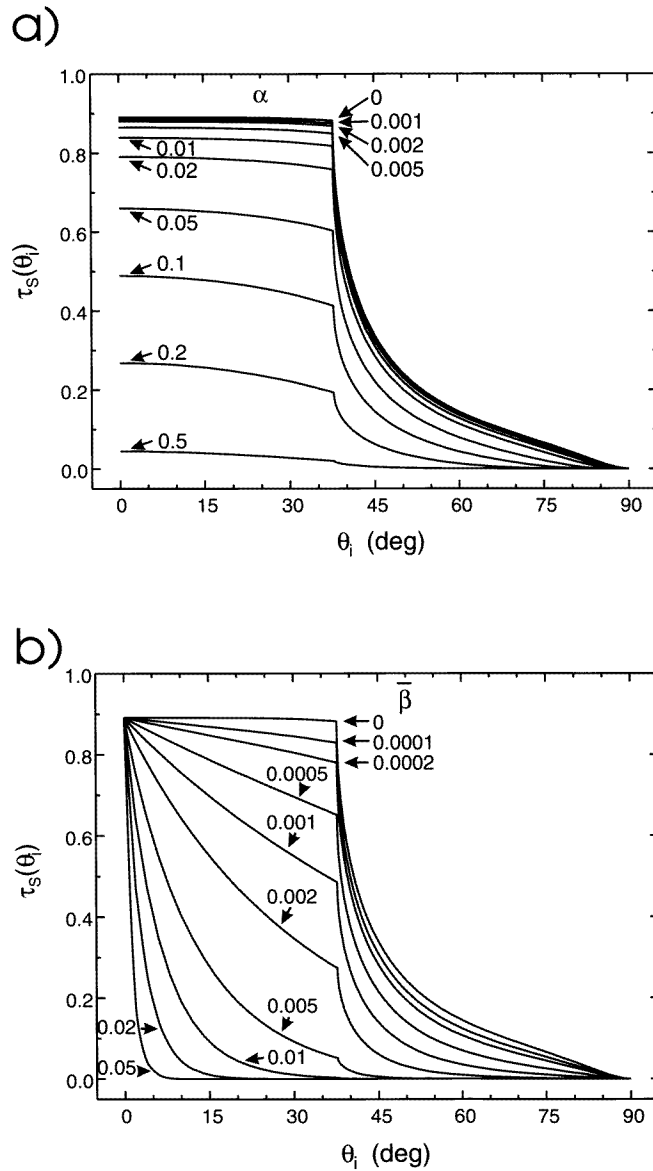


**Figure 7.** The results of the skew ray hypothesis calculated using equation (11), (a) for different values of  $\alpha$ , assuming  $\bar{\beta} = 0$ , and (b) for different values of  $\bar{\beta}$ , assuming  $\alpha = 0$ . The calculations were performed using  $L = 6$  mm,  $n_1 = 1.62$ , and  $n_2 = 1.50$ , giving an optical fibre with  $NA = 0.61$ . The values of  $\alpha$  are given in  $\text{mm}^{-1}$ .

### 3. Experimental procedure and results

#### 3.1. Lenses

Using equation (6), the limiting meridional angle ( $\theta_{i,M}$ ) was calculated as a function of  $f$ -number and demagnification ( $m$ ). These data are shown in figure 8. Using equation (1),

the coupling efficiency of lenses was calculated for various limiting meridional angles. These calculations, shown in figure 9, were performed for lenses coupled to a hypothetical Lambertian light source and a phosphor screen. The angular emission of light from the phosphor screens has been measured experimentally using a goniometer-mounted radiometer and has been described previously (Maidment and Yaffe 1995). The results for the phosphor screen shown in figure 9 were calculated using the angular emission model (Maidment and Yaffe 1995) for a phosphor screen coated with an overcoat material. The results are valid for phosphor screens with values of  $k_p t = 0.5$  (Min-R regular and medium, Eastman Kodak, Rochester, NY) to  $k_p t = 0.7$  (Lanex regular or medium, Eastman Kodak, Rochester, NY). One can calculate the expected coupling efficiency of any lens and most phosphor screens by combining the data in figures 8 and 9 with an appropriate value of  $\tau$  (typically 0.7–0.9).

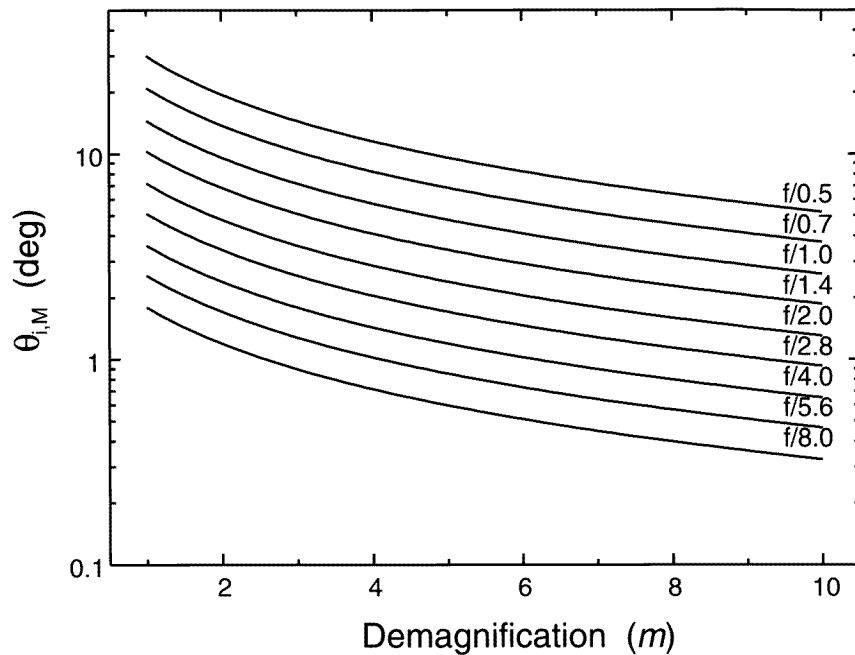


**Figure 8.** The effect of demagnification and  $f$ -number on acceptance half angle ( $\theta_{i,M}$ ).

### 3.2. Fibre optics

As described in subsection 2.3, the meridional and skew ray models predict an angular dependence of the optical-fibre transmission efficiency. The validity of these models for calculating the coupling efficiency of the FO faceplates and tapers used in POC detectors was evaluated by measuring the angular-dependent radiance of a nearly Lambertian light source (Rowlands *et al* 1989), with and without an FO output window. The transmission efficiency of the fibre optics was calculated by taking the ratio of the radiance at each angle with and without the FO faceplate. As defined in subsection 2.2.3, the transmission efficiency of a fused faceplate includes the reduction of light transmission accounted by the fractional area of the core glass.

The results of two such experiments are shown in figure 10. Each of the FO faceplates

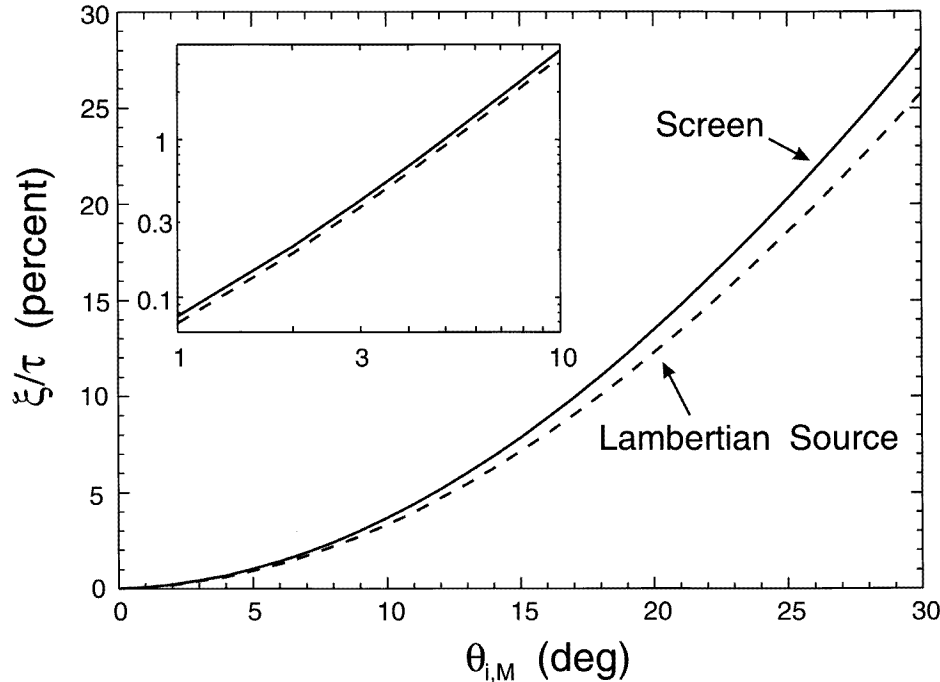


**Figure 9.** The effect of acceptance half angle ( $\theta_{i,M}$ ) on the geometric component of the optical coupling efficiency. The data are replotted in the inset graph to aid the reader.

consists of  $6\ \mu\text{m}$  diameter fibres, 6 mm long. The packing efficiency,  $A = 0.80 \pm 0.03$ . The core glass had a refractive index of  $n_1 = 1.60$  and the cladding glass had a refractive index of  $n_2 = 1.49$ . The faceplates were suspended in air, thus  $n_i = n_o = 1.0$ ,  $\text{NA} = 0.6$ , and  $\theta_{i,M} = 35^\circ$ , similar to the fibres simulated and discussed in figures 5 and 7. One FO faceplate contained EMA material; the other did not. The angular-dependent radiance emitted from the light source was measured using a goniometer described previously (Maidment and Yaffe 1995) for angles of  $\theta_o$  between  $0^\circ$  and  $70^\circ$ . The measurements were repeated with each of the two FO faceplates mounted in the exit port of the light source. Each FO faceplate was  $1\ \text{cm} \times 3\ \text{cm}$ , which represents about 0.5% of the area of the integrating sphere, and is sufficiently small to not affect the angular distribution of light within the sphere (Kingslake 1983, p 114). Thus the light incident upon the input surface of the FO faceplate was approximately Lambertian. The ratio of the radiance of the light incident upon each FO faceplate to the radiance of the light transmitted through the faceplate was used to determine  $\tau(\theta)$  for each FO faceplate. The average RMS measurement error was 1.4%.

The measured data, shown in figure 10, are compared to data calculated using the meridional model equation (9) and the skew ray model equation (11). In the meridional and skew ray models, it was assumed that  $\alpha = 0.001\ \text{mm}^{-1}$ , and  $\beta = 0.0003$ . These values provide the best fit of the data for angles below the limiting meridional angle ( $\sim 35^\circ$ ) when the data are simultaneously fitted to the transmission efficiency of the two FO faceplates using a linear least-squares method. These values are typical of those of similar fibre optics.

To determine the coupling efficiency of various FO assemblies, the limiting meridional angle,  $\theta_{i,M}$ , was calculated as a function of NA and demagnification ( $m$ ) assuming  $n_i = 1.0$ .

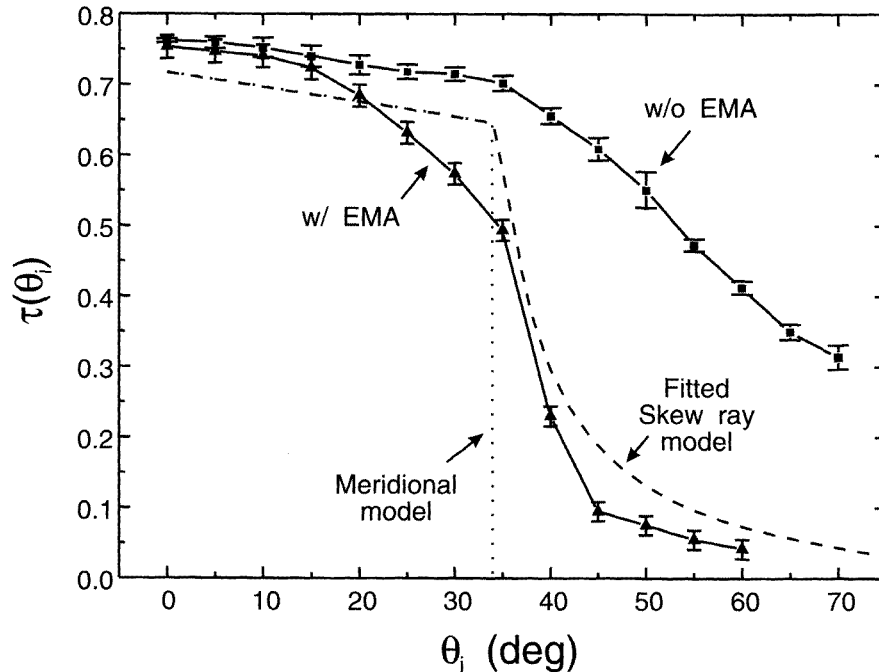


**Figure 10.** The transmission efficiency of two FO faceplates measured as a function of angle. The faceplates were identical with the exception of the presence of EMA. A comparison between experimental and theoretical results is shown. The theoretical results are given for the meridional model (equation (9)), and the skew ray model (equation (11)).

These data are shown in figure 11. Using equation (1), the FO coupling efficiency was then calculated for a range of values of  $\theta_{i,M}$ . These calculations were performed for FO assemblies coupled to a Lambertian source, and for the angular emission of light emitted from a phosphor screen using the model described above. An ideal FO, with  $\alpha = \beta = 0$ , and a 'real' FO, with  $\alpha$  and  $\beta$  as derived from the fitted data above, were modelled. In figure 12, the coupling efficiency calculated using the meridional model of the transmission efficiency given by equation (9) is shown. In figure 13, the coupling efficiency calculated using the skew ray model of the transmission efficiency given by equation (11) is shown.

## 4. Discussion

### 4.1. Lenses

As shown in figure 8, both increased demagnification and increased  $f$ -number result in lower values of  $\theta_{i,M}$ . In figure 9, the coupling efficiency of lenses is shown for varying values of the limiting meridional angle. These data were calculated for a Lambertian light source and several phosphor screens. There is less than a 1% difference in the coupling efficiency of light emitted at a given limiting angle for the various phosphor screens modelled. However, for limiting angles less than  $30^\circ$ , the lens coupling efficiencies are 10% greater for light emitted from a phosphor screen than from a Lambertian source (i.e. uniform radiance), because the phosphor screens produce light for which the radiance is more forward directed

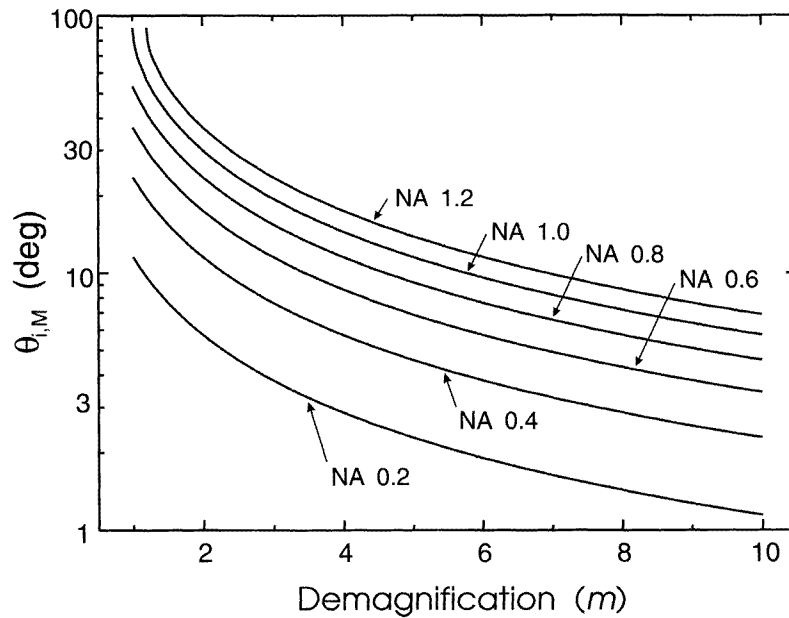


**Figure 11.** The effect of demagnification and NA on acceptance half angle ( $\theta_{1,M}$ ), assuming  $n_i = 1.0$ .

(Maidment and Yaffe 1995). Thus, the common assumption that the angular emission of light from a phosphor screen can be treated as Lambertian will result in underestimation of the optical coupling efficiency.

#### 4.2. Fibre optics

A comparison of the measured and calculated angular dependences of the FO transmission efficiency, shown in figure 10, demonstrates a decrease in transmission efficiency near the limiting meridional angle which is likely to be due to scattering within the fibre and fibre wall non-uniformities. In the fibre optics without EMA, the transmission efficiency appears to be much greater. However, this increased transmission of light is due to 'flare', the transmission of light by processes other than total internal reflection. Such flare will reduce contrast in the resulting images. These observations are consistent with the work of Kapany (1967), who states that the transmission efficiency models fail when there is coupling between fibres of FO assemblies (i.e. cross-talk), when there is conduction of light in the cladding, or when there are imperfections that cause scattering or diffraction.

By the nature of their manufacture, both of the measured FO faceplates contained a mixture of circular and irregularly shaped fibres. When viewed microscopically ( $\times 600$ ), it was observed that  $75 \pm 5\%$  of the fibres were circular, with the remainder being hexagonal, tear-drop shaped, or square. Skew rays will be preserved by the circular fibres; however the skew rays with  $\theta_1 > \theta_{1,M}$  will not undergo guided transmission in irregularly shaped fibres since the skew angle,  $\gamma$ , is not conserved. The transmission efficiency should, therefore, be bounded in the lower limit by the results of the meridional ray model and in the upper limit by the results of the skew ray analysis, as observed in figure 10.

The limiting meridional angles for various optical fibres are shown in figure 11. In

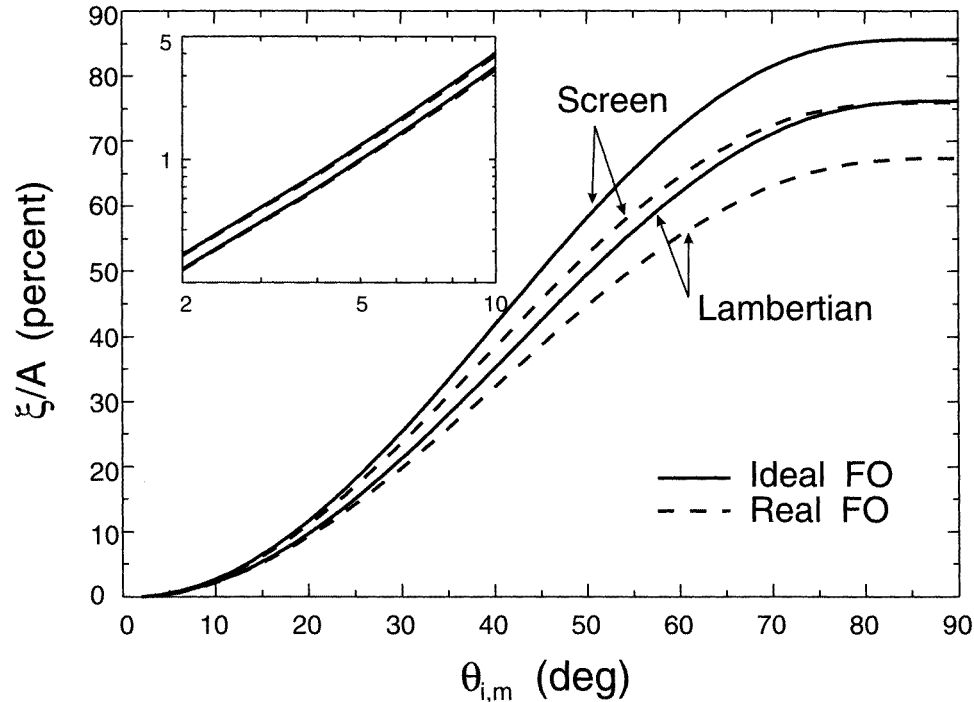


**Figure 12.** The effect of acceptance half angle ( $\theta_{i,M}$ ) on optical coupling efficiency assuming the meridional model of transmission efficiency, without consideration of the fractional active area ( $A$ ). The data are replotted in the inset graph to aid the reader.

a similar result to that of lenses, increased demagnification or decreased NA results in a smaller value of  $\theta_{i,M}$ . The optical coupling efficiency is shown assuming the meridional model of the transmission efficiency in figure 12, and assuming the skew ray model in figure 13. For the meridional model, there was less than a 1% difference in coupling efficiency between the phosphor screens, but there was nearly a 20% difference between the phosphor screens and the Lambertian source at small angles, and 12% at large angles. There was virtually no difference for transmission efficiency between the ideal and real fibre optics at small angles; however for fibre optics with limiting meridional angles greater than about  $30^\circ$  an 8–12% reduction in coupling efficiency was observed in the real fibre optics.

For the skew ray model, a similar relationship between phosphor screens and Lambertian sources was observed. There was also a similar relationship between the values of transmission efficiency between the real and the ideal fibre optics. However, when the skew ray data are compared to the meridional data, greater differences are evident. For fibre optics with limiting meridional angles of approximately  $30^\circ$  the skew ray model predicts a nearly 50% increase in transmission efficiency as compared to the meridional model. Also, the values of transmission efficiency plateau at a smaller limiting angle in the skew model than in the meridional model. The presence of these systematic differences between the meridional and skew ray models of transmission efficiency indicates that the true angular transmission efficiency should be measured to obtain accurate estimates of photometric efficiency with fused FO assemblies.

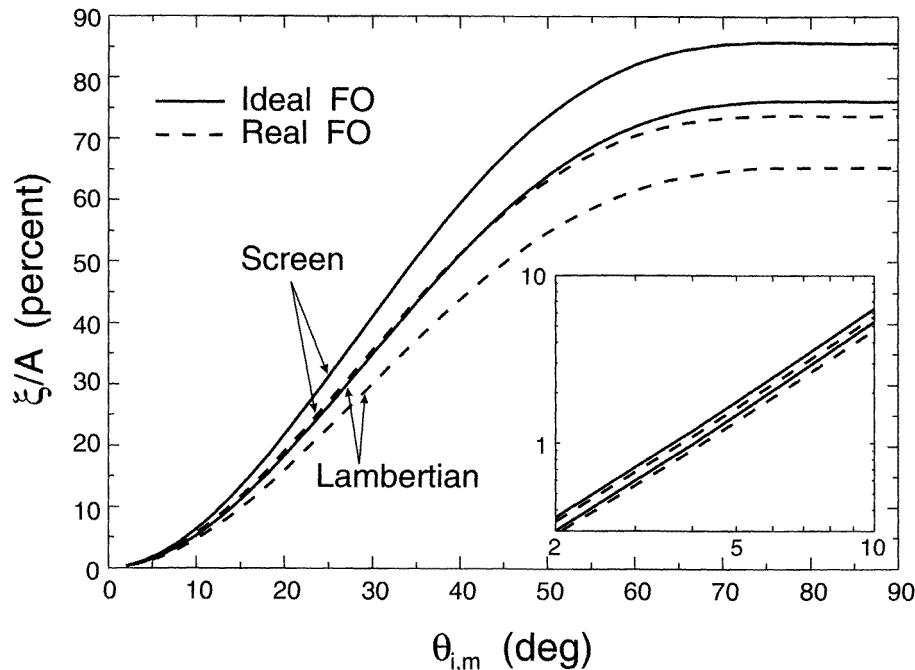


**Figure 13.** The effect of acceptance half angle ( $\theta_{i,m}$ ) on optical coupling efficiency assuming the skew ray model of transmission efficiency without consideration of the fractional active area ( $A$ ). The data are replotted in the inset graph to aid the reader.

## 5. Conclusions

We have presented methods for calculating and measuring the number of quanta at various stages in optically coupled detectors and the related coupling efficiencies. Those aspects of fundamental optics that contribute to the calculation of coupling efficiency in lenses and fibre optics have been reviewed. In the case of a phosphor screen coupled by lenses with limiting angles of less than  $30^\circ$ , we calculated that the coupling efficiency will be 10% greater than estimated for a Lambertian source. Similar differences are observed when a phosphor screen is coupled to a fibre optic. The differences occur because a phosphor screen typically produces light which is more forward directed than a Lambertian source.

In the case of fibre optics, an angular-dependent value of transmission efficiency is required to estimate optical coupling efficiency accurately. The models of Kapany and Capellaro (1961) and Potter (1961) were compared to experimentally measured results. In the absence of flare, the two models provide the lower and upper limits of transmission efficiency, respectively. The effect of EMA on the transmission efficiency of FO faceplates has been demonstrated. In instances in which accurate photometry is required, the angular-dependent emission of the light source and the angular-dependent transmission of the fibre optic should be measured.

## Acknowledgments

We gratefully acknowledge the support of the Medical Research Council of Canada and the National Cancer Institute of Canada.

## References

- Albrecht C 1965 Noise sources in image intensifying devices *Diagnostic Radiological Instruments: Modulation Transfer Function* ed R D Moseley and J H Rust (Springfield, IL: Thomas)
- Andre M P, Spivey B A, Tran J, Martin P J and Kimme-Smith C M 1994 Small-field image-stitching approach to full-view digital mammography *Radiology* **193**(P) 253
- Born M and Wolf E 1989 *Principles of Optics* 6th edn (New York: Pergamon)
- Boyd R W 1983 *Radiometry and the Detection of Optical Radiation* (New York: Wiley) pp 82–4
- Dugas J, Sotom M, Martin L and Cariou J M 1987 Accurate characterization of the transmittivity of large-diameter multimode optical fibres *Appl. Opt.* **26** 4198–208
- Fu T Y 1984 Information transfer efficiency of x-ray image intensifier based imaging systems *PhD Dissertation* University of Arizona
- Jenkins F A and White H E 1957 *Fundamentals of Optics* 3rd edn (New York: McGraw-Hill) pp 154–7
- Kapany N S 1955 Optical systems with flexible axes *PhD Dissertation* Imperial College
- 1967 *Fiber Optics: Principles and Applications* (New York: Academic)
- Kapany N S and Capellaro D F 1961 Fiber optics. VII. Transfer from Lambertian emitters *J. Opt. Soc. Am.* **51** 23–31
- Karellas A, Harris L J, Liu H, Davis M A, and D'Orsi C J 1992 Charge-coupled device detector: performance for small-field mammographic imaging applications *Med. Phys.* **19** 1015–23
- Kingslake R 1983 *Optical System Design* (New York: Academic)
- Li Y F and Lit J W Y 1985 Transmission properties of a multimode optical-fiber taper *J. Opt. Soc. Am. A* **2** 462–8
- Liu H, Karellas A, Harris L J and D'Orsi C J 1994 Methods to calculate the lens efficiency in optically coupled CCD x-ray imaging systems *Med. Phys.* **21** 1193–5
- Maidment A D A 1993 Scanned-slot digital mammography *PhD Dissertation* University of Toronto
- Maidment A D A and Yaffe M J 1994 Analysis of the spatial-frequency-dependent DQE of optically-coupled digital mammography detectors *Med. Phys.* **21** 721–9
- 1995 Analysis of signal propagation in optically-coupled detectors for digital mammography: I. Phosphor screens *Phys. Med. Biol.* **40** 877–89
- Maidment A D A, Yaffe M J, Plewes D B, Mawdsley G E, Soutar I C and Starkoski B G 1993 Imaging performance of a prototype scanned-slot digital mammography system *Proc. SPIE* **1986** 93–103
- Miller L D 1971 Transfer characteristics and spectral response of television camera tubes *Photoelectronic Imaging Devices* vol 1, ed L M Biberman and S Nudelman (New York: Plenum) pp 282–90
- Munro P, Rawlinson J A and Fenster A 1990 A digital fluoroscopic imaging device for radiotherapy localization *Int. J. Radiat. Onc. Biol. Phys.* **18** 641–9
- Nishikawa R M and Yaffe M J 1990 Effect of various noise sources on the detective quantum efficiency of phosphor screens *Med. Phys.* **17** 887–93
- Okashi T 1982 *Optical Fibers* (New York: Academic)
- Potter R J 1960 A theoretical and experimental study of optical fibers *PhD Dissertation* University of Rochester
- 1961 Transmission properties of optical fibers *J. Opt. Soc. Am.* **51** 1079–89
- Potter R J, Donath E and Tynan R 1963 Light-collecting properties of a perfect circular optical fiber *J. Opt. Soc. Am.* **53** 256–60
- Rabbani M, Shaw R and VanMetter R 1987 Detective quantum efficiency of imaging systems with amplifying and scattering mechanisms *J. Opt. Soc. Am. A* **4** 895–901
- Rabbani M and VanMetter R 1989 Analysis of signal and noise propagation for several imaging mechanisms *J. Opt. Soc. Am. A* **6** 1156–64
- Rowlands J A, Schulenburg K S and DeCrescenzo G 1989 A light source for testing radiological television cameras *Med. Phys.* **16** 1–6
- Swindell W 1991 The lens coupling efficiency in megavoltage imaging *Med. Phys.* **18** 1152–3
- Ter-Pogossian M M 1967 *The Physical Aspects of Diagnostic Radiology* (New York: Harper and Row)
- VanMetter R and Rabbani M 1990 An application of multivariate moment-generating functions to the analysis of signal and noise propagation in radiographic screen–film systems *Med. Phys.* **17** 65–71

Vermeulen A J W A, Beekmans A A G and Haarman J W 1982 Design and functional description of optical image distributors for image intensifier systems *Acceptance Testing of Radiological Imaging Equipment* ed P J P Lin *et al* (New York: American Institute of Physics) pp 29–44